RSC Advances

PAPER

View Article Online
View Journal | View Issue

Cite this: *RSC Adv.*, 2015, **5**, 31826

Evaluation of the dynamic electrochemical stability of ionic liquid–metal interfaces against reactive oxygen species using an *in situ* electrochemical quartz crystal microbalance†

Chunhui Xiao,‡ Abdul Rehman and Xiangqun Zeng*

Received 8th January 2015
Accepted 11th March 2015

DOI: 10.1039/c5ra00396b

www.rsc.org/advances

The dynamic interactions between the electrochemically generated superoxide radical ($O_2^{\bullet-}$) and three structurally different ionic liquids (ILs) were characterized using an electrochemical quartz crystal microbalance (EQCM). We established the long-term stability of the interface (on the scale of hours and weeks) against the most ubiquitous interferent in electrochemical energy devices and sensors: oxygen. Oxygen potentially limits the application of IL electrolytes in these devices. In particular, the electrochemical behavior of the $O_2/O_2^{\bullet-}$ couple and the ion pair formed between the cation of an IL and $O_2^{\bullet-}$ were evaluated. $O_2^{\bullet-}$ tends to form ion pair complexes with the cation of an IL, subsequently abstracting a proton to form different products depending on the cationic structure of the IL used. The reversibility of the $O_2/O_2^{\bullet-}$ electrode reaction depends on the subsequent chemical reactions between $O_2^{\bullet-}$ and the IL, which are more pronounced at slow scan rates. It was found that $O_2^{\bullet-}$ was significantly more stable in the IL with the [BMPY] cation than in ILs with imidazolium salts. The stability of the ILs towards $O_2^{\bullet-}$ attack follows the order [BMPY][NTf_2] > [BdMIM][NTf_2] > [BMIM][NTf_2] as evaluated on a time-scale of a few seconds to minutes and up to 3 weeks. It was found that the formation of the [Cation]$\cdots O_2^{\bullet-}$ ion pair complex lowers the local viscosity of the IL near the electrode, reflected in the change in the oscillating frequency of the quartz crystal electrode. As much as is the feasibility for the formation of this ion pair, that much is the tendency of the IL to lose its electrochemical stability. A combined analysis can provide a quick indication of the dynamic stability of the electrode–electrolyte interface for any IL in the presence of certain electrochemical reactions using the EQCM technique.

Introduction

The electrode–electrolyte interface has a central role in electrochemical devices, including those devices that involve energy production and storage and those that are used as sensors. Ionic liquids (ILs)[1] provide a range of options to diversify this interface as a result of their structural heterogeneity and synthetic flexibility. As a consequence, they have attracted much interest[2–7] in recent years, especially in the demanding energy sectors of dye-sensitized fuel cells,[6,8] batteries[9–11] and supercapacitors,[12–14] as well as in fundamental electrochemistry.[15–18] However, it is very important to understand and quantify the stability of this interface in the presence of species that are ubiquitous under ambient conditions. Oxygen is one of these species, presence of which in many of these electrochemical reactions can generate reactive oxygen species. The superoxide radical ($O_2^{\bullet-}$) affects subsequent reactions and the stability of the interface. Therefore the thermodynamics, kinetics and even the mechanisms of the electrode reactions are changed, compromising the efficiency of the overall process. For example, recent work[19] has shown that the mechanism of CO_2 reduction at IL interfaces is very different in the presence and absence of oxygen. The study further showed that modification of the reaction mechanism occurs because of the competition between CO_2 and the cations of the ILs reacting with the electrochemically generated $O_2^{\bullet-}$ radical. This modification was shown to be dependent on the structure of the IL, indicating that oxygen affects the interface of different ILs to varying degrees. A dynamic measurement of subtle variations at the electrode–IL interface is therefore critical in ensuring that all these applications work, which, in turn, requires a more sophisticated methodology to quantify the effects than simple electrochemical techniques.

Unlike in conventional organic solvents, the redox peaks of the $O_2/O_2^{\bullet-}$ couple in ILs are asymmetrical in shape, with the characteristics of a typical steady-state condition. This is a result

Department of Chemistry, Oakland University, Rochester, Michigan 48309, USA. E-mail: zeng@oakland.edu

† Electronic supplementary information (ESI) available: Fig. S1–S6 as noted in the text are provided. See DOI: 10.1039/c5ra00396b

‡ Present address: School of Science, Xi'an Jiaotong University, Xi'an, China.

of the specific interactions of $O_2^{\bullet-}$ with the cation of the ILs.[20–22] As superoxide has a negative charge and the electronic spin density is delocalized between the two oxygen atoms, it can act as a powerful nucleophile in aprotic solvents.[23–25] This property has also been observed in ILs. For example, the superoxide generated *in situ* in ILs based on the imidazolium cation tends to attack positively charged organic cations, leading to strong ion pairing of the $O_2^{\bullet-}\cdots[Cation]^+$.[26,27] The ion pairing phenomenon during the dioxygen reduction reaction in EMI^+-based ILs has been thoroughly investigated.[28] It was observed that, in DMSO solution, the degree of association of $O_2^{\bullet-}$ with the EMI^+ cation is comparable with that of $O_2^{\bullet-}$ with H_2O. However, as the degree of association in pure ILs is much stronger, such an ion pairing may ultimately lead to the abstraction of a proton from the cation to form $HO_2^{\bullet-}$ and carbine, or other types of compounds,[29–31] thus hampering the stability of the $O_2^{\bullet-}$ species in the ILs. The cation structure in an IL plays an important part in this regard. Islam *et al.*[32] reported that $O_2^{\bullet-}$ can attack the 2-position of the imidazolium ring to form an ion pair complex. Eventually, the ion pair complex of the imidazolium cation and the $O_2^{\bullet-}$ species undergoes a ring-opening reaction to form hydrogen peroxide. AlNashef *et al.*[33] reported that $O_2^{\bullet-}$ can react with alkyl imidazolium cations to yield 2-imidazolones. Hayyan *et al.*[22] studied the generation of $O_2^{\bullet-}$ in pyridinium-, morpholinium-, ammonium- and sulfonium-based ILs by cyclic voltammetry (CV) and chronoamperometry. They found that $O_2^{\bullet-}$ is not stable in the pyridinium-based ILs, but is stable in the other ILs for the duration of the experiments. However, most experiments were performed to observe the stability of the superoxide at very short time-scales (from seconds to minutes) depending on the methods and techniques used. However, none of these studies estimated the stability of the ILs involved at the longer time-scales that are important in the real-world applications of these systems. In many of these studies, simulation models were used to fit the experimental parameters to obtain mechanistic information.

In contrast, we and others have shown[19,34,35] that the use of an *in situ* electrochemical quartz crystal microbalance (EQCM) provides a better and powerful method to characterize the structure and dynamics of the properties of the IL–electrode interface, allowing real-time monitoring of variations in the surface populations during electrochemically driven redox reactions. The electrified interface causes the IL ions to rearrange, thereby generating different kinds of solvent polarization effects depending on the IL used, which determines the reaction rate. The high viscosity and resulting slow relaxation dynamics of ILs[36] allow the time-scale of these polarization effects and the electron transfer processes to be at similar levels, thus allowing the measurement of subtle variations in the structure of the IL solvent during the redox reaction. The results can then be used to quantify the ionic interactions *via* adsorption on the electrode surface, ion pairing within the IL or with the reaction products, and the ionic arrangements. The data generated in this way (Scheme 1) enable us to account for different types of structural orientations under potential control during the electrochemical perturbation of the IL–electrode interface. Therefore it is thought that this approach may give an insight into various fundamental aspects of IL stability against

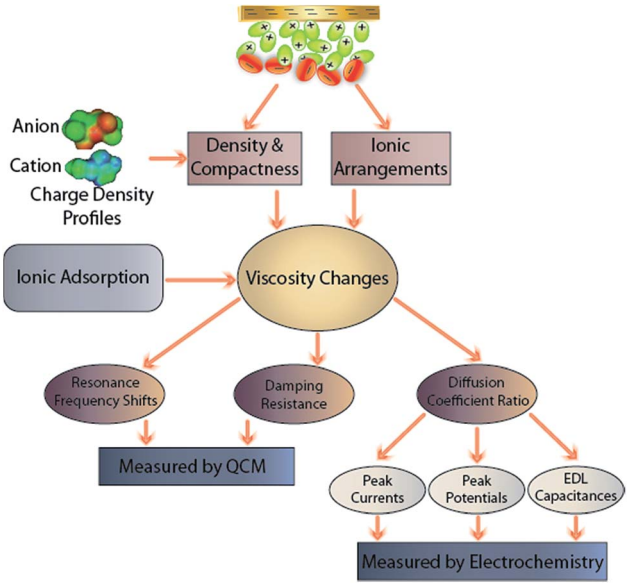

Scheme 1 Flow chart of the dynamic variables influenced by the structural heterogeneities in ILs as well as by their reactions with electrochemically generated species. These variables affect each other during electrochemical perturbations and can be detected by the EQCM system.

certain species such as the $O_2^{\bullet-}$ radical and the dynamics of redox reactions in ILs.

In this work, the dynamic interactions between the electrochemically generated superoxide radical ($O_2^{\bullet-}$) and ILs with different structures were characterized by the EQCM approach to quantitatively estimate their stability against this radical. Specifically, we studied the interactions between the electro-generated superoxide and the ILs with two new focuses. First, we were motivated to characterize the reactivity of the *in situ* generated superoxide anion radicals in ILs at much longer time-scales (seconds to hours) by multiple cycles of CV and at various scan rates to quantitatively determine the stability of ILs in the presence of superoxide anion radicals. Second, we intended to demonstrate that the EQCM technique can measure the dynamics of the potential-induced subtle variations at an IL–electrode interface in the absence and presence of oxygen redox processes. The key emphasis is to understand how the IL structural heterogeneity of the interface contributes to the reaction kinetics by selectively interacting with the superoxide radical. Cumulatively, these analyses can provide new quantitative information regarding the oxygen reduction reaction (ORR) in ILs. This is important for the selection and design of new and stable electrolytes and for the utilization of $O_2^{\bullet-}$ in a wide range of applications, such as developing highly selective electrochemical sensors and electrochemical energy storage devices using ILs.

Experimental

Chemicals

Hydrophobic 1-butyl-3-methylimidazolium bis(trifluoromethanesulfonyl)imide ([BMIM][NTf_2]), 1-butyl-2,3-dimethylimidazolium bis(trifluoromethanesulfonyl)imide ([BdMIM][NTf_2]) and 1-

butyl-1-methylpyrrolidinium bis(trifluoromethanesulfonyl) imide ([BMPY][NTf_2]) with purities of 99% were purchased from Ionic Liquids Technologies (USA). All the ILs were dried before use in the electrochemical experiments by heating to 120 °C in a vacuum oven for a minimum of 12 h until no visible signs of water were present in the IR spectrum (CaF_2 plates). All other chemicals were purchased from Sigma-Aldrich (St. Louis, MO, USA) and were of analytical-reagent grade and used without further purification.

Electrochemical measurements

Volumes of 100 μL of the respective ILs were drop-coated onto the working electrode inside a Kel-F electrochemical cell designed to facilitate the correct positioning of the three-electrode system. An Au quartz crystal (AT-cut 10 MHz, unpolished with an approximately 1000 Å thick Au film with an area of 0.23 cm^2; International Crystal) was used as the working electrode. Just before use, the Au substrates were cleaned by a freshly prepared "piranha" solution for about 30 s and subsequently rinsed with excess amounts of water, ethanol and acetone, then dried under nitrogen gas (**caution**: the "piranha" solution, 1 : 3 H_2O_2 : H_2SO_4, reacts violently with many organic materials and should be used with extreme care; it should not be stored in a sealed container). A platinum wire and a silver wire (0.5 mm diameter) were used as the counter electrode and the quasi-reference electrode, respectively. They were mechanically polished prior to use to remove the oxide film, rinsed with acetone and then dried under vacuum. The distance from the tip of the two electrodes to the center of the working electrode was set at 2 mm to minimize the effects of uncompensated electrolyte resistance. All potentials were measured using Fc/Fc^+ (50 μM ferrocene in ILs) as the internal reference. Prior to the measurements, the entire system was dried in a vacuum oven at 60 °C for at least 2 h to remove any water and other impurities. The total gas flow was fixed at 200 sccm by digital mass flow controllers (MKS Instruments). Two mass flow controllers were used to adjust the volume ratio of the test gas flows. The highly purified gases (N_2 and O_2) were used containing <10 ppm water as described by the manufacturers. All the gas analytes were prepared by pre-mixing the gases in a 500 mL glass bottle with a stirring fan and then connecting to a drying column consisting of silica gel and solid calcium chloride before their introduction into the electrochemical cell. Using this drying process, the water level could be limited to <10 ppm. The gas was run for at least 12 h to ensure that equilibrium was established before the measurements were made. The IL system was purged constantly during the experiments with dry nitrogen or a mixture of nitrogen and oxygen to prevent any trace amounts of water or other impurities. All experiments were performed inside a Faraday cage and at room temperature (23 ± 1 °C).

EQCM measurements

The electrical admittance curve of the QCM was measured with an Agilent 4395A network/spectrum/impedance analyzer (Agilent Technologies, USA). Simultaneous electrochemical measurements were made using a CHI 1000A electrochemical workstation (CH Instruments, USA). A 1 μF capacitor was connected between the working electrode and the Agilent impedance analyzer to minimize the instrumental interference between the potentiostat and the Agilent impedance analyzer. The QCM was allowed to resonate for at least 2 h at the initial conditions for a baseline signal and then various potential programs were applied for the electrochemical measurements. The Agilent analyzer was preferred over other routinely used frequency measuring devices (*e.g.* RQCM) for QCM data monitoring because the IL–electrode interface is much more viscous than traditional aqueous electrolytes. In such a scenario, damping of the oscillation wave is so high that a more sophisticated instrument is required to maintain the crystal oscillation and obtain the correct data.

Results and discussion

Generation of superoxide anion radicals in ILs

The superoxide radical was first generated by the electrochemical reduction of oxygen in all three ILs ([BMIM][NTf_2], [BdMIM][NTf_2] and [BMPY][NTf_2]) and was examined at the Au QCM electrode by CV to analyze the stability of the ILs. Fig. 1 shows that the resulting peaks for oxygen reduction and superoxide oxidation were observed at negative potentials compared with those in a nitrogen atmosphere (inset). The cathodic peak between −1.2 and −1.3 V was assigned to the one-electron reduction of O_2 to $O_2^{\bullet -}$ whereas the anodic peak between −1.2 and −1.0 V was the subsequent oxidation of $O_2^{\bullet -}$:

$$O_2 + e^- \rightleftharpoons O_2^{\bullet -} \quad (1)$$

The presence of the $O_2^{\bullet -}$ oxidation peak provides evidence that the $O_2^{\bullet -}$ generated *in situ* is chemically stable within the time-scale of experiments in the three ILs studied. These results are consistent with those reported previously.[22,26,37–40]

It is necessary to determine the concentration of O_2 in each IL for quantitative evaluation. In this study, the concentration of O_2 (C) and its diffusion coefficient (D) were determined by a chronoamperometric technique with both macro- and ultra-

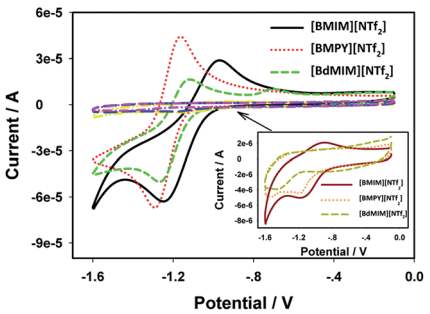

Fig. 1 Second potential cycle cyclic voltammograms of the three ILs in the absence and presence of 40 vol% oxygen. Inset: enlarged scale in the absence of oxygen. Scan rate = 100 mV s^{-1}. Nitrogen was used as the dilution gas.

micro disk electrodes. For the macro-disk electrode, when a sufficient over-potential is applied, the current density is inversely proportional to the square root of time, as represented by Cottrell's equation:

$$i(t) = \frac{nFAD^{1/2}C}{\pi^{1/2}t^{1/2}} \quad (2)$$

where n and F are the number of electrons and Faraday's constant, respectively. The steady-state current, i_{ss}, for the ultra-micro disk electrode with a radius r_0 is given by the following equation:

$$i_{ss} = 4nFDCr_0 \quad (3)$$

thus D and C can be calculated from the values of $D^{1/2}C$ and DC can be obtained for the macro- and ultra-micro disk electrodes, respectively. Table 1 summarizes the diffusion coefficient, D, and concentration of O_2, together with the viscosity, for the three ILs studied.

It is clear from Table 1 that the order of magnitude for the oxygen concentration is [BdMIM][NTf_2] > [BMPY][NTf_2] > [BMIM][NTf_2]. However, as can be seen from the results of the EQCM experiments, [BdMIM][NTf_2], with the highest oxygen concentration, has the lowest peak current for superoxide oxidation. The frequency change in this IL was also the smallest among the three ILs studied. This indicates that, in this viscous electrolyte system, D might play a more significant part in the ORR than the concentration. For this reason, we addressed the contributions from D in more detail. As shown in Fig. 1, the cathodic reduction peak current (i_{pc}) in [BdMIM][NTf_2] is lower than that in the other two ILs, as it has an extremely small D value, close to one-quarter of that in [BMIM][NTf_2]. The similarity of i_{pc} in both [BMPY][NTf_2] and [BMIM][NTf_2] is a result of their close values of D and C. The solubility of oxygen in [BMPY][NTf_2] is higher than that in [BMIM][NTf_2], but the diffusion of O_2 in [BMIM][NTf_2] is faster. Note that the order of the anodic superoxide oxidation peak current (i_{pa}) in the three ILs is different from i_{pc}, with the following order: $i_{pa,[BMPY][NTf_2]} > i_{pa,[BMIM][NTf_2]} > i_{pa,[BdMIM][NTf_2]}$. The anodic peak potential (E_{pa}) also shows a significant difference. For example, E_{pa} in [BMIM][NTf_2] is shifted by about 300 mV positive compared with other two ILs. The change in the superoxide oxidation processes can be explained as an EC_{rev} mechanism in which one-electron oxygen reduction is followed by the reversible formation of an ion pair $O_2^{\bullet-}\cdots[Cation]^+$ as proposed by Compton and coworkers:[26,27]

$$O_2 + e^- \rightleftharpoons O_2^{\bullet-} + [Cation]^+ \rightleftharpoons O_2^{\bullet-}\cdots[Cation]^+ \quad (4)$$

The rapid ion pairing of $O_2^{\bullet-}\cdots[Cation]^+$ hampers the superoxide oxidation process, causing a positive shift in the potential and leading to an increased peak-to-peak separation (ΔE_p), making it more electrochemically irreversible than expected for a simple E process. The extent of irreversibility depends on the kinetics of the coupled chemical processes.

Experiments with the $O_2/O_2^{\bullet-}$ couple were performed in three ILs at varying scan rates (detailed data are given in Fig. S1†) to further investigate the relationship between the stability of the superoxide and the structure of the ILs. Fig. 2 shows the variations in i_{pc}, i_{pa}, E_{pc}, E_{pa} and ΔE_p when the scan rates were varied. The peak currents were proportional to the square root of the scan rate for all three ILs. This shows that the reduction of O_2 and the oxidation of $O_2^{\bullet-}$ in the ILs are diffusion-controlled. E_{pc} shifted to a more negative value and E_{pa} shifted to a more positive value with increasing scan rates.

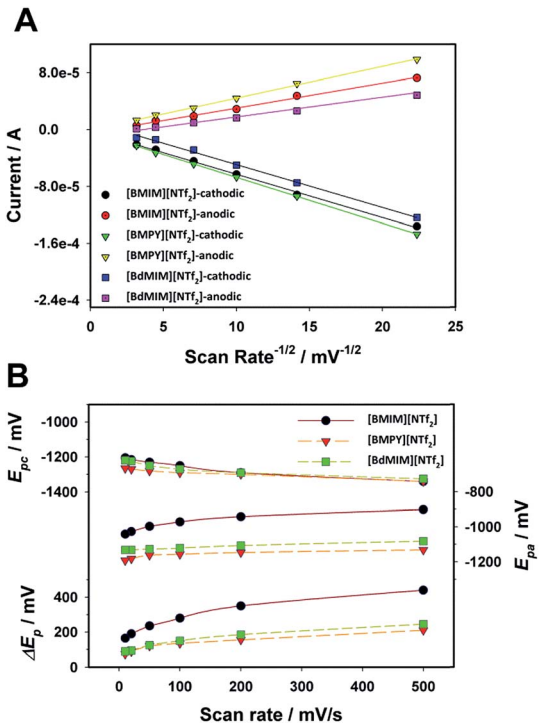

Fig. 2 Plot of (A) i_{pc} and i_{pa} and (B) E_{pc}, E_{pa} and ΔE_p *versus* the scan rate in three ILs in the presence of oxygen (40 vol%) at the second potential cycle. The dilution gas was nitrogen.

Table 1 Diffusion coefficient (D) and saturated concentration (C) of oxygen (40 vol%) in three ILs; the viscosity (η) and conductivity of the ILs are also listed[a]

	D (O_2) ($m^2\ s^{-1}$)	C [O_2] (mM)	η[41] (cP)	Conductivity[42] (mS cm^{-1})
[BMIM][NTf_2]	1.8×10^{-10}	4.3	52	3.7
[BMPY][NTf_2]	1.1×10^{-10}	7.1	89	2.4
[BdMIM][NTf_2]	4.8×10^{-11}	9.4	105	2.2

[a] Viscosity and conductivity data were measured at 20 °C.

This is characteristic of a quasi-reversible system. The E_{pa} shows notable differences among the three different ILs studied, but E_{pc} remains at a relatively constant value, reflecting the different degrees of association between the electro-generated superoxide and the cation. The uncompensated resistance (iR_u) and surface reaction kinetics at the metal electrodes were used to explain the variation in the ΔE_p of the $O_2/O_2^{\bullet-}$ redox couple in different aprotic solvents.[37,43] However, the ΔE_p values of the oxygen redox processes in these three ILs follows the order: $\Delta E_{p,[BMIM][NTf_2]} \gg \Delta E_{p,[BdMIM][NTf_2]} > \Delta E_{p,[BMPY][NTf_2]}$. The broadest ΔE_p peak can be observed in $[BMIM][NTf_2]$, but the uncompensated resistance (iR_u) in $[BMIM][NTf_2]$ should be the lowest as its conductivity is the highest of the three ILs. Thus the variation in ΔE_p is mainly attributed to the variation in the electrode reaction kinetics in different ILs and there may be an effect from iR_u, although this is too small to have a significant effect. The variation in electrode reaction kinetics were the results of the (bond-forming) ion paring $O_2^{\bullet-}\cdots[Cation]^+$, which leads to a positive shift in E_{pa} as well as an increase in ΔE_p. The stronger the interactions between $O_2^{\bullet-}$ and the cation, the larger the value of ΔE_p. The formation of the ion pair is probably a result of both electrostatic interactions and hydrogen bonding between the $O_2^{\bullet-}$ and the $[Cation]^+$. It has long been known that all three of the imidazolium ring protons (C2, C4 and C5) are acidic, although the proton in the C2 position is the most acidic. $[BdMIM]^+$ has fewer protons at the C2 position of the ring, which makes it a weaker hydrogen bond donor than $[BMIM]^+$. As the ability to donate hydrogen bonds increases with the increasing s-character of the C–H bond, imidazolium-based ILs commonly have a higher hydrogen bond acidity than pyrrolidinium- and alkyl ammonium-based ILs.

Multiple cycles of CV to characterize superoxide stability in ILs

The kinetics of forming $O_2^{\bullet-}\cdots[Cation]^+$ ion pairs has been reported as a reversible reaction in which $O_2^{\bullet-}$ can be stabilized in ILs. Several groups have identified that such ion pairing promotes the $O_2^{\bullet-}$ species to eventually abstract protons from the imidazolium cation to form hydrogen peroxide and a new product:[32,33]

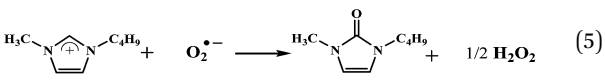

(5)

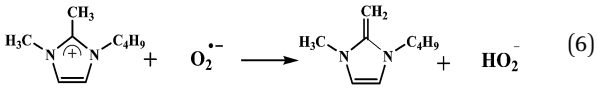

(6)

Note that these reactions are irreversible, thus the long-term stability of ILs against this radical anion still needs to be investigated. For this purpose, the reversibility of the $O_2/O_2^{\bullet-}$ redox couple in the ILs was further investigated by multiple cycles of CV at various scan rates.

Fig. 3 shows the data for the continuous cycling (20 cycles) of the oxygen redox process in three ILs at fast (500 mV s^{-1}) and slow (10 mV s^{-1}) scan rates (other scan rates are shown in Fig. S2†). The i_{pc} gradually decreased with increasing numbers of scan cycles. This is explained based on two factors: (1) the decrease in the double-layer charging current in subsequent cycles; and (2) the depletion of oxygen as a result of the redox processes of $O_2/O_2^{\bullet-}$, as oxygen cannot be rapidly supplied from the bulk ILs to the electrode interface. Several interesting trends were observed for i_{pa}. For example, i_{pa} remains almost constant in both $[BMIM][NTf_2]$ and $[BMPY][NTf_2]$ at 500 mV s^{-1}. It decreases with each subsequent scan cycle in $[BdMIM][NTf_2]$. A small intermediate peak at about −0.7 for the oxidation of $O_2^{\bullet-}$ and hydrogen peroxide (H_2O_2) to O_2 is observed; a similar phenomenon has been reported by other workers.[32] At a scan rate of 10 mV s^{-1}, the i_{pa} in $[BMIM][NTf_2]$ and $[BdMIM][NTf_2]$ dramatically decreases, whereas i_{pa} decreases very slowly in $[BMPY][NTf_2]$. In addition, compared with a scan rate of 500 mV s^{-1}, a new small anodic peak at about −0.4 V at a scan rate of 10 mV s^{-1} was observed in $[BMIM][NTf_2]$ (Fig. 3D), which is assigned to the oxidation of HO_2^-.[32] The enlarged view of this potential region in three ILs is shown in Fig. S3.† A smaller peak at about −0.4 V can be observed in $[BdMIM][NTf_2]$, but is hardly seen in $[BMPY][NTf_2]$, re-confirming that the abstraction of protons from $[BMIM][NTf_2]$ is easiest among the three selected ILs, followed by $[BdMIM][NTf_2]$ and $[BMPY][NTf_2]$.

Therefore the reversibility of the $O_2/O_2^{\bullet-}$ redox couple in the three ILs is different under different conditions (scan rate, cycle number), suggesting that the stability of the superoxide depends on the structure of the ILs. The significant irreversibility observed in the multiple CV experiments at slower scan rates indicates that the kinetics of the ion pairing and subsequent chemical reactions are slow, which can be observed more clearly at slower scan rates. At slow scan rates some of the $O_2^{\bullet-}\cdots[Cation]^+$ ion complex can form H_2O_2 and other compounds (*e.g.* 2-imidazolones). Thus a mechanism of homogeneous chemical reactions (including reversible ion pair formation and an irreversible protonation process) coupled to the electron transfer process of oxygen can be summarized as follows:

$$O_2^{\cdot-} + [Cation]^+ \rightleftharpoons O_2^{\cdot-}\cdots[Cation]^+ \xrightarrow{\text{protonation}} H_2O_2 + \text{other product} \quad (7)$$

The quantitative diagnosis of chemical reactions coupled with electrode reactions is often based on the relative current heights of the anodic and cathodic peaks. If the conversion of the ion pair complex to H_2O_2 is a slow process, at fast potential scan rates most of the $O_2^{\bullet-}$ will be oxidized back to O_2, thus the value of i_{pa}/i_{pc} will be close to 1. If the conversion of the ion pair complex to H_2O_2 is fast, some of the $O_2^{\bullet-}$ will be lost to this process. Less $O_2^{\bullet-}$ will be available for oxidation back to O_2 on the backward potential scan and therefore the anodic peak will be smaller and the value of i_{pa}/i_{pc} will be <1. The i_{pa}/i_{pc} values of three ILs at the fifth cycle were plotted as a function of scan rate (Fig. 4). Note that the i_{pa} and i_{pc} values were achieved using the

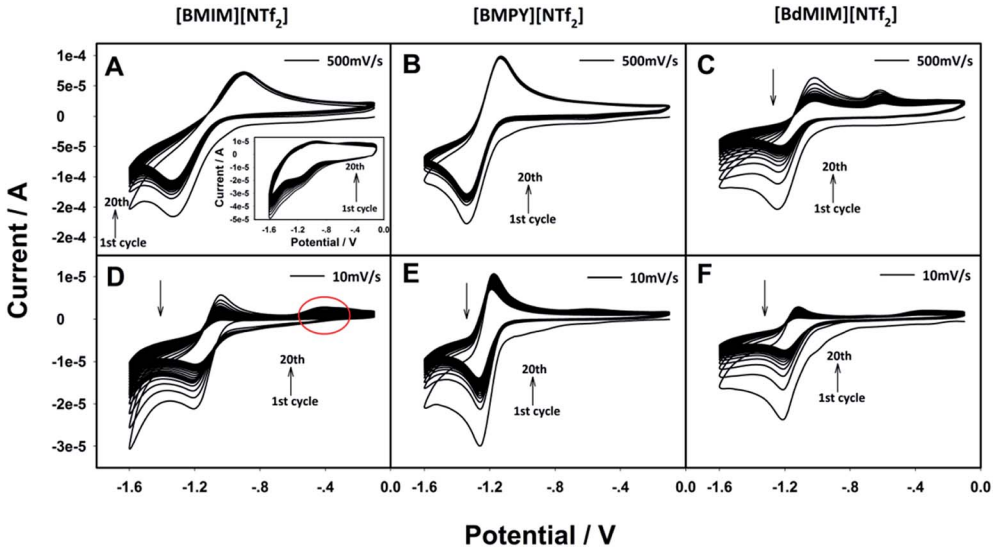

Fig. 3 Twenty typical cycles of CV at different scan rates of (A–C) 500 mV s^{-1} and (D–F) 10 mV s^{-1} in three ILs in the presence of oxygen (40 vol%). Inset: CV in nitrogen without oxygen. Nitrogen was used as the dilution gas.

CHI 1040A electrochemical analyzer software after subtraction of the background current. In addition, the main anodic peak of about −1.1 V is about 13 times larger than that of the peak at about −0.7 V in [BdMIM][NTf_2]. Therefore we believe that the effect of this intermediate peak is very small to be negligible. The trends of the plots are similar for [BdMIM][NTf_2] and [BMIM][NTf_2] in which i_{pa}/i_{pc} decreases at fast scan rates with increasing scan rate, although, at slow scan rates, i_{pa}/i_{pc} increases with increasing scan rates. The value of i_{pa}/i_{pc} showed the least change in [BMPY][NTf_2], but a slight decrease in i_{pa}/i_{pc} can still be observed at scan rates <20 mV s^{-1}, even in this IL.

Nicholson and Shain[44] reported that the general trend followed by the peak current ratio as a function of scan rate can serve as a quick diagnosis for electrochemical mechanisms involving coupled chemical reactions. At fast scan rates the oxygen reduction process is an E_rC_r mechanism with a reversible electron transfer (E_r) followed by a reversible chemical reaction (C_r) (eqn (4)). At slow scan rates the reaction is changed to a mechanism of a reversible electron transfer (E_r) followed by an irreversible chemical (C_i) reaction (E_rC_i mechanism), corresponding to ion pair formation and further protonation processes during the following superoxide reaction in the IL (eqn (7)). Fig. 5 compares the change in i_{pa}/i_{pc} at various scan rates with the increase in the number of cycles in three ILs. The change in the i_{pa}/i_{pc} value in ILs at different scan cycles is an indicator of the loss in the reversibility of the redox process with time. The smallest change in i_{pa}/i_{pc} observed in [BMPY][NTf_2] indicates that the stability of the $O_2^{\bullet-}$ in this IL is more than 100 min. The most striking result is in [BMIM][NTf_2], where i_{pa}/i_{pc} shows a large change at 30 min at scan rates of 20 and 10 mV s^{-1} (if we convert the CV scans to a time-scale, the 20 cycles for these two scan rates are equivalent to 50 and 100 min, respectively). The change in i_{pa}/i_{pc} could be seen in [BdMIM][NTf_2], although it is much smaller than that of [BMIM][NTf_2], showing the varying stability of the superoxide radical in different ILs. In summary, the rate of reaction between the $O_2^{\bullet-}$ and the cation of the ILs follows the order [BMIM][NTf_2] > [BdMIM][NTf_2] > [BMPY][NTf_2]. This order is consistent with the result obtained from the ΔE_p value.

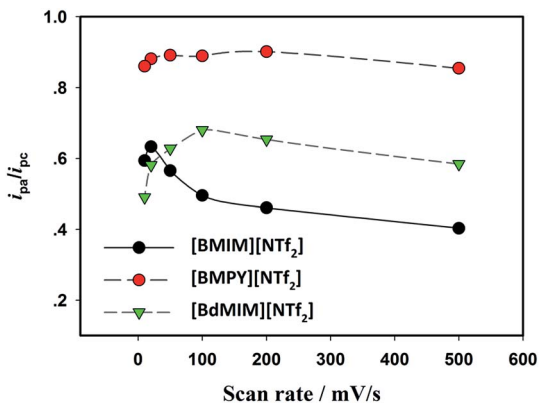

Fig. 4 Variations in the i_{pa}/i_{pc} for the fifth cycle with different scan rates in three ILs in the presence of oxygen (40 vol%). Nitrogen was used as the diluting gas.

EQCM evaluation of the ORR in ILs

To further investigate the effect of oxygen reduction in ILs, an EQCM method was used. The QCM integrated with electrochemical methods enabled us to obtain dynamic QCM data as a function of time and as a function of the electrochemical processes, thereby providing a framework for understanding how the ionic structures and populations changed while the potential was scanned from the anodic to the cathodic directions and *vice versa*. The EQCM technique can thus trace the time-resolved variations at the IL–electrode interface that are often too subtle to be detected with spectroscopic techniques (*i.e.* measuring the orientation of the ions at specified potentials

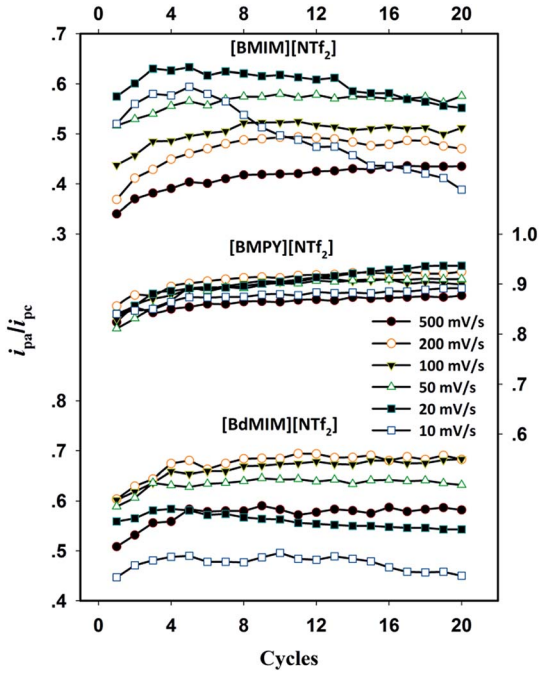

Fig. 5 Variations in the values of i_{pa}/i_{pc} in each CV cycle at different scan rates in three ILs in the presence of oxygen (40 vol%). Nitrogen was used as the dilution gas.

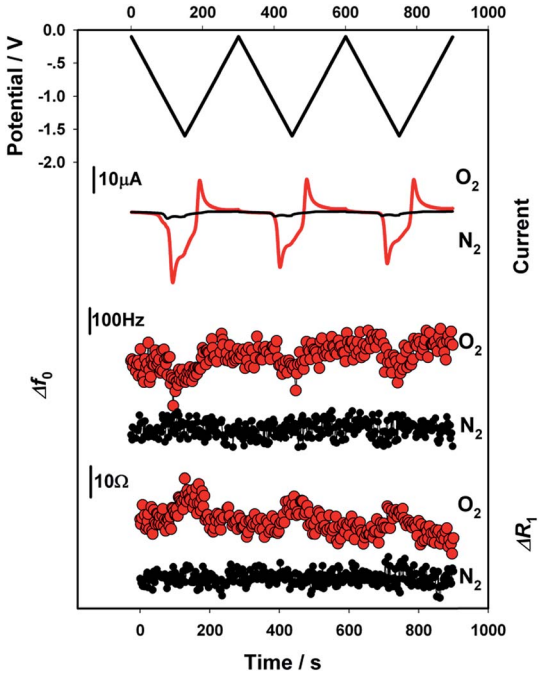

Fig. 6 Simultaneous recording of potential, current, Δf_0 and ΔR_1 during three cycles of CV in [BMPY][NTf$_2$] in the absence and presence of oxygen (40 vol%). Scan rate = 10 mV s^{-1}. Nitrogen was used as the dilution gas. The momentary and reversible decrease in frequency during the reduction reaction of oxygen is caused by the small variations at the electrode surface that accompany the redox process (the electroactive species may diffuse to the depletion layer from a balanced state to either an oxidized or reduced state).

only). Using this analysis for our system, we could experimentally monitor changes in several physical parameters related to the IL–electrode interface during the electron transfer process of the $O_2/O_2^{\bullet-}$ couple and its subsequent chemical reactions. Fig. 6 shows the simultaneous responses of changes in potential, current, oscillation frequency (Δf_0) and damping resistance (ΔR_1) for [BMPY][NTf$_2$], both in the presence and absence of oxygen as obtained from the EQCM experiments. A decrease in frequency during the oxygen reduction process in the cathodic potential scan and an increase in frequency during the superoxide oxidation process at the anodic potential scan were observed. However, no obvious change in frequency was observed under pure N_2 conditions for same experimental conditions, suggesting that the potential polarization does not generate significant changes in the electrode–electrolyte interface. This kind of EQCM response is also observed during the electrode reaction of $[Fe(CN)_6]^{4-}$ and $[Fe(CN)_6]^{3-}$ in aqueous solution, which has been explained as small variations (<3%) in the density and viscosity of the depletion layer that accompany the oxidation or reduction of the electroactive species.[45] We also observed this in [BMPY][NTf$_2$] during the redox process of ferrocene (Fig. S4†). If we assume that the mass transport of O_2 during its redox process is slow in the ILs, so that it contributes little to the frequency change, the frequency waves that are very closely related to the CV current curves should be assigned to the change in the viscosity and density of the electrolyte near the electrode surface resulting from molecular interactions between the superoxide and the ILs. At an applied negative potential, it has been reported that, in an IL, the electrode has a surface charge that is over-screened by a monolayer of counter ions (cations); a balancing excess of opposite ions (anions) exists in the next layer to counter the over-screening.[46] The increase in applied potential also causes this effect to be spread out over a larger number of ion pairing layers.[47,48] However, these rearrangements as a result of potential cycling between 0 and −1.6 V are fully reversible and do not cause obvious changes in viscosity near the electrode, reflected in the flat frequency curve obtained with nitrogen alone. There is a shift in frequency after the electron transfer process in the presence of oxygen, observable in all three ILs, but with different amplitudes of frequency changes (Fig. S5†). Thus the reduction of O_2 to $O_2^{\bullet-}$ in the IL results in a spectacular dissimilarity in the diffusion coefficients between O_2 and $O_2^{\bullet-}$, undergoing large conformational or solvation changes after electron transfer. The difference in their interaction with the ILs contributes to the change in the density and viscosity of the depletion layer.

Martin *et al.*[49] reported a series of equivalent circuit parameters and a modified Butterworth–Van Dyke equivalent electrical circuit for the characterization of a QCM with simultaneous mass and liquid loading. The values of $|\Delta f_0/\Delta R_1|$ allow the separation of the mass and viscosity effects for the frequency signals. For a 10 MHz quartz crystal, if $|\Delta f_0/\Delta R_1|$ is larger than 11.6 Hz Ω^{-1}, then the frequency changes can be ascribed predominantly to the mass effect. In the case of oxygen reduction, for both the waves for a single cycle and the overall trend after three cycles, the $|\Delta f_0/\Delta R_1|$ ratios are smaller than

11.6 Hz Ω^{-1}, confirming that the QCM response is mainly due to viscosity changes at the interface.

The $O_2^{\bullet-}$ generated couples with the cation of an IL near the electrode surface to form an ion pair complex, which is not completely reversible, as discussed earlier, and is hypothesized to lower the local viscoelasticity near the electrode, leading to the change in oscillating frequency (Scheme 2). In general, by consideration of the similar structures in ILs, the differences in viscosity are mainly influenced by hydrogen bonding and van der Waals interactions.[50,51] In this case, $O_2^{\bullet-}$ as a hydrogen bonding acceptor interacts with the cation and competes with the anion for the proton. This leads to [Cation]$\cdots O_2^{\bullet-}$ ion pairing, thereby suppressing the hydrogen bonding in ILs. This is expected to reduce the viscosity as a result of weakened interactions between the cation and anion.[50]

The decay length, δ, which describes the approximate thickness of the electrolyte and electrode interface, the effective change of which is sensed by the EQCM, is limited by a function of the density and viscosity of the solution as follows:[45]

$$\delta = \eta^{1/2}/(\pi f_0 \rho)^{1/2} \quad (8)$$

The EQCM response appears to be governed essentially by the cation in the diffusion layer near the negatively electrified electrode surface and the ion pairing force between the cation and $O_2^{\bullet-}$. Fig. 7A demonstrates simultaneously the recorded frequency changes over a total of 20 CV cycles, sweeping in the selected ILs in the presence of oxygen (40 vol%) at a scan rate of 20 mV s^{-1}. In the range of selected ILs, we observed distinct variations in the changes in f_0 generated by potential cycling. It is clearly seen that the order of magnitude for the total change in Δf_0 is [BMIM][NTf_2] (602.4 Hz) > [BMPY][NTf_2] (303.4 Hz) > [BdMIM][NTf_2] (178.4 Hz). A flat frequency curve was observed in [BMIM][NTf_2] in the absence of oxygen, as in the other two ILs (data not shown), indicating that the QCM response can be ascribed to the ORR. [BMIM][NTf_2] presents the highest change in f_0 as it combines the maximum diffusion coefficient with the strongest intensity of ion pairing. [BdMIM][NTf_2] presents the lowest f_0 response because of its minimum diffusion coefficient dominates over the moderate ion pairing force. The numerical values of the resulting Δf_0 before and after CV sweeping in each IL with different potential cycling scan rates are shown in Fig. 7B. Surprisingly, when the scan rate was higher than or

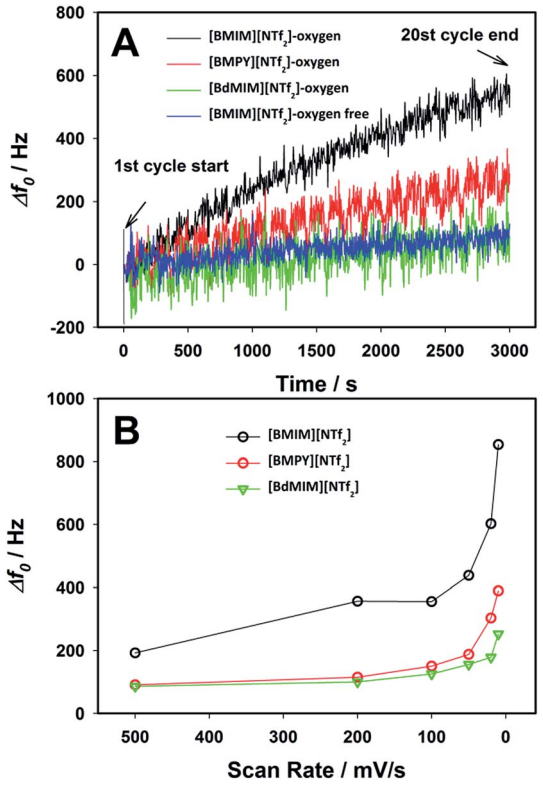

Fig. 7 (A) Simultaneously recorded frequency of 20-cycle CV scans in three ILs in the absence and presence of oxygen (40 vol%) at a scan rate of 20 mV s^{-1} and (B) total increase in frequency after 20 scan cycles at different scan rates (10–500 mV s^{-1}) in three ILs in the presence of oxygen (40 vol%). Nitrogen was used as the dilution gas. The overall effect of the [Cation]$\cdots O_2^{\bullet-}$ ion pairing is a decrease in viscosity, thereby increasing the overall frequency of the QCM. This effect is irreversible and probably due to the interface reactions that led to the viscoelastic property changes at the Au–IL interface.

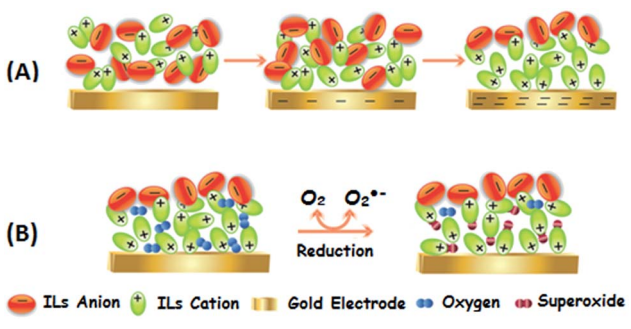

Scheme 2 Schematic illustration of the ionic arrangement with (A) increasingly negative potential and (B) the formation of ion pairs in ILs.

equal to 100 mV s^{-1}, suggesting that the oxygen reduction as well as the reactivity of the superoxide with ILs was reversible, the frequency was essentially unchanged. However, at slower scan rates, when there is a longer period of negative potential polarization causing more and more cation layers to be gathered near the electrode surface, an increase in the local concentration of the cation is expected, which can lead to a higher possibility of forming ion pairs and thus a higher EQCM response. This was exactly the case when the scan rates were less than or equal to 50 mV s^{-1}, with significantly higher values of Δf_0 as a result of the stronger and irreversible reactivity of the superoxide with the ILs. These results further confirmed our previous hypothesis that the QCM response during oxygen reduction comes from the viscosity and density changes resulting from the formation of the ion pair complex. The smaller dependence between the QCM response and the scan rate (>50 mV s^{-1}) denies another possibility that QCM response comes from the mass loading, such as the adsorption of superoxide or other intermediate compounds, as more adsorbate will be produced at slower scan rates and therefore the frequency due to mass loading should decrease rather than increase. The other type of variations seen in the frequency

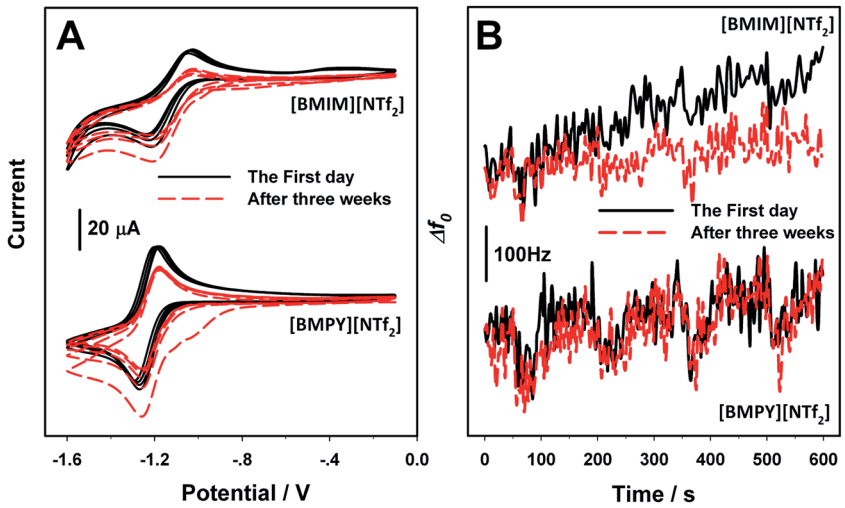

Fig. 8 (A) Four-cycles of CV and (B) simultaneously recorded changes in Δf_0 for [BMIM][NTf_2] and [BMPY][NTf_2] on the first day and after 3 weeks in the presence of oxygen (40% v/v). Scan rate = 20 mV s^{-1}. Nitrogen was used as the dilution gas.

curves is the kind of frequency wave produced during each cycle of the measurement, which provides an indication of the stability of the superoxide anion as related to the electrochemical data. This wave is clearly visible in the case of the ferrocene couple (Fig. S4†), where there is no overall increase in frequency and the direction of the frequency shift changes fairly coherently with the direction of the potential scan. This frequency wave is also observable for [BMPY][NTf_2], even for the 20th cycle (Fig. 7A). This indicates that the superoxide is consistently being re-oxidized, lessening the ion pairing effect during the anodic scan and reversing the direction of the shift in frequency. In contrast, this kind of wave is only visible in the first few cycles for [BMIM][NTf_2], after which only an increase in the overall frequency is seen. This shows that the $O_2^{\bullet-}$ generated has more irreversible interactions within this IL. [BdMIM][NTf_2] lies between these two, further supporting the results obtained *via* electrochemical measurements for the long-term stability of $O_2^{\bullet-}$ in different ILs. Thus, by combining the two results, the long-term stability of the $O_2^{\bullet-}$ in ILs can be determined *in situ* in several electrochemical reactions.

Long-term stability of the IL–electrode interface in the presence of $O_2^{\bullet-}$

The long-term stability of ILs in the presence of electrochemically generated $O_2^{\bullet-}$ was determined in independent experiments at a much longer time-scale than the CV experiments using the EQCM method. We performed the CV experiment for the ORR every day without changing the ILs and the EQCM data were collected. Fig. 8A shows the EQCM results of oxygen reduction in the ILs at the first day and at the 21st day. The i_{pa}/i_{pc} value in [BMIM][NTf_2] significantly decreased to about 37.3 ± 1.6% from its initial value. This change is much bigger than that in [BMPY][NTf_2] (15.1 ± 2.3%). Furthermore, the simultaneously recorded frequency shows significant variations (Fig. 8B). There is a noticeable difference in [BMIM][NTf_2], reflecting a decrease of about 160 Hz in the frequency after potential cycling. However, the frequency curves almost completely overlapped in [BMPY][NTf_2]. As discussed earlier, ion pairing may ultimately lead to the $O_2^{\bullet-}$ species abstracting the proton from the IL cations, especially from the imidazolium-based ILs, to form carbine and H_2O_2. However, it has been shown that peroxide species can be oxidized to H_2O in ILs. In this instance, H_2O moisture as a proton source plays a greater part in the acceleration of the protonation reaction of the $O_2^{\bullet-}$ species. The existence of a proton source leads to the spontaneously rapid protonation of the electro-generated superoxide species, thus lowering the ion pairing effect and the reversibility of the O_2 redox reaction. These results demonstrate that ILs containing [BMPY] offer a superior long-term stability for $O_2^{\bullet-}$ attack than imidazolium salts.

Conclusions

The ORR frequently interferes with electrochemical energy conversion reactions and sensors and is also a critical factor in the use of ILs for such applications. This is a result of its potential to disrupt the stability of ILs and to modify the reaction mechanisms. We investigated the ORR in this new class of electrolytes by an EQCM approach in three structurally different ILs. Our results showed that the electro-generated $O_2^{\bullet-}$ couples with the cations of the ILs to form ion pair complexes. The reversibility of the $O_2/O_2^{\bullet-}$ reaction, which reflects the extent of the formation of ion pairs, decreases at slow scan rates. The degree of ion pairing strongly depends on the cation of the ILs. The [BMIM]-based ILs tend to form the strongest ion pairs with the superoxide radical, followed by the [BdMIM]- and [BMPY]-based ILs. The formation of the [Cation]$\cdots O_2^{\bullet-}$ ion pairs was proved to lower the local viscosity of the electrolyte near the electrode, reflected by the oscillating frequency change of the QCM measurements. The stability of the ILs in the presence of the *in situ* generation of $O_2^{\bullet-}$ was characterized. It was found that the IL containing [BMPY] offered a superior long-term

stability for $O_2^{\bullet-}$ attack compared with those based on imidazolium salts.

The principles obtained from this work can be extended to other redox processes in ILs. The results from this study allow the relationship between the structure of ILs and their chemical stability towards $O_2^{\bullet-}$ to be characterized, which is important for the selection and design of new and stable electrolytes and for further utilization of $O_2^{\bullet-}$ in many applications. This study also established that EQCM is an effective tool to investigate the redox reaction at the IL–electrode interface. Work is in progress to use the EQCM technique to study different types of electron transfer reaction in various ILs.

Acknowledgements

X. Zeng thanks the Office of Naval Research for support (Grant N000141010734).

References

1 A. Rehman and X. Q. Zeng, *Acc. Chem. Res.*, 2012, **45**, 1667–1677.
2 J. N. Barisci, G. G. Wallace, D. R. MacFarlane and R. H. Baughman, *Electrochem. Commun.*, 2004, **6**, 22–27.
3 J. Ding, D. Zhou, G. Spinks, G. Wallace, S. Forsyth, M. Forsyth and D. MacFarlane, *Chem. Mater.*, 2003, **15**, 2392–2398.
4 S. T. Handy, *Chem.–Eur. J.*, 2003, **9**, 2938–2944.
5 M. P. Jensen, J. Neuefeind, J. V. Beitz, S. Skanthakumar and L. Soderholm, *J. Am. Chem. Soc.*, 2003, **125**, 15466–15473.
6 P. Wang, S. M. Zakeeruddin, J.-E. Moser and M. Grätzel, *J. Phys. Chem. B*, 2003, **107**, 13280–13285.
7 C. Yang, Q. Sun, J. Qiao and Y. Li, *J. Phys. Chem. B*, 2003, **107**, 12981–12988.
8 S. M. Zakeeruddin and M. Grätzel, *Adv. Funct. Mater.*, 2009, **19**, 2187–2202.
9 C. J. Allen, S. Mukerjee, E. J. Plichta, M. A. Hendrickson and K. M. Abraham, *J. Phys. Chem. Lett.*, 2011, **2**, 2420–2424.
10 V. Chakrapani, F. Rusli, M. A. Filler and P. A. Kohl, *J. Phys. Chem. C*, 2011, **115**, 22048–22053.
11 S.-L. Chou, J.-Z. Wang, J.-Z. Sun, D. Wexler, M. Forsyth, H.-K. Liu, D. R. MacFarlane and S.-X. Dou, *Chem. Mater.*, 2008, **20**, 7044–7051.
12 Y. Lauw, M. D. Horne, T. Rodopoulos, A. Nelson and F. A. M. Leermakers, *J. Phys. Chem. B*, 2010, **114**, 11149–11154.
13 M. Anouti, L. Timperman, M. el hilali, A. Boisset and H. Galiano, *J. Phys. Chem. C*, 2012, **116**, 9412–9418.
14 T. Y. Kim, H. W. Lee, M. Stoller, D. R. Dreyer, C. W. Bielawski, R. S. Ruoff and K. S. Suh, *ACS Nano*, 2010, **5**, 436–442.
15 M. C. Buzzeo, R. G. Evans and R. G. Compton, *ChemPhysChem*, 2004, **5**, 1106–1120.
16 D. R. MacFarlane, M. Forsyth, P. C. Howlett, J. M. Pringle, J. Sun, G. Annat, W. Neil and E. I. Izgorodina, *Acc. Chem. Res.*, 2007, **40**, 1165–1173.
17 D. R. MacFarlane, J. M. Pringle, P. C. Howlett and M. Forsyth, *Phys. Chem. Chem. Phys.*, 2010, **12**, 1659–1669.
18 M. J. A. Shiddiky and A. A. J. Torriero, *Biosens. Bioelectron.*, 2011, **26**, 1775–1787.
19 C. H. Xiao and X. Q. Zeng, *J. Electrochem. Soc.*, 2013, **160**, H749–H756.
20 M. C. Buzzeo, O. V. Klymenko, J. D. Wadhawan, C. Hardacre, K. R. Seddon and R. G. Compton, *J. Phys. Chem. A*, 2003, **107**, 8872–8878.
21 M. Hayyan, F. S. Mjalli, I. M. AlNashef and M. A. Hashim, *Int. J. Electrochem. Sci.*, 2012, **7**, 9658–9667.
22 M. Hayyan, F. S. Mjalli, M. A. Hashim and I. M. AlNashef, *Ind. Eng. Chem. Res.*, 2012, **51**, 10546–10556.
23 H. Gampp and S. J. Lippard, *Inorg. Chem.*, 1983, **22**, 357–358.
24 D. T. Sawyer, G. Chiericato, C. T. Angelis, E. J. Nanni and T. Tsuchiya, *Anal. Chem.*, 1982, **54**, 1720–1724.
25 D. T. Sawyer and J. S. Valentine, *Acc. Chem. Res.*, 1981, **14**, 393–400.
26 A. S. Barnes, E. I. Rogers, I. Streeter, L. Aldous, C. Hardacre, G. G. Wildgoose and R. G. Compton, *J. Phys. Chem. C*, 2008, **112**, 13709–13715.
27 E. I. Rogers, X.-J. Huang, E. J. F. Dickinson, C. Hardacre and R. G. Compton, *J. Phys. Chem. C*, 2009, **113**, 17811–17823.
28 M. M. Islam and T. Ohsaka, *J. Phys. Chem. C*, 2008, **112**, 1269–1275.
29 D. Méry, J. R. Aranzaes and D. Astruc, *J. Am. Chem. Soc.*, 2006, **128**, 5602–5603.
30 T. L. Amyes, S. T. Diver, J. P. Richard, F. M. Rivas and K. Toth, *J. Am. Chem. Soc.*, 2004, **126**, 4366–4374.
31 A. Marcinek, J. Zielonka, J. Gębicki, C. M. Gordon and I. R. Dunkin, *J. Phys. Chem. A*, 2001, **105**, 9305–9309.
32 M. M. Islam, T. Imase, T. Okajima, M. Takahashi, Y. Niikura, N. Kawashima, Y. Nakamura and T. Ohsaka, *J. Phys. Chem. A*, 2009, **113**, 912–916.
33 I. M. AlNashef, M. A. Hashim, F. S. Mjalli, M. Q. A.-h. Ali and M. Hayyan, *Tetrahedron Lett.*, 2010, **51**, 1976–1978.
34 A. R. Hillman, *J. Solid State Electrochem.*, 2011, **15**, 1647–1660.
35 L. Yu, Y. Huang, X. Jin, A. J. Mason and X. Zeng, *Sens. Actuators, B*, 2009, **140**, 363–370.
36 H. Y. Lee, J. B. Issa, S. S. Isied, E. W. Castner, Y. Pan, C. L. Hussey, K. S. Lee and J. F. Wishart, *J. Phys. Chem. C*, 2012, **116**, 5197–5208.
37 S. O'Toole, S. Pentlavalli and A. P. Doherty, *J. Phys. Chem. B*, 2007, **111**, 9281–9287.
38 M. T. Carter, C. L. Hussey, S. K. D. Strubinger and R. A. Osteryoung, *Inorg. Chem.*, 1991, **30**, 1149–1151.
39 R. G. Evans, O. V. Klymenko, S. A. Saddoughi, C. Hardacre and R. G. Compton, *J. Phys. Chem. B*, 2004, **108**, 7878–7886.
40 Y. Katayama, H. Onodera, M. Yamagata and T. Miura, *J. Electrochem. Soc.*, 2004, **151**, A59–A63.
41 X.-J. Huang, E. I. Rogers, C. Hardacre and R. G. Compton, *J. Phys. Chem. B*, 2009, **113**, 8953–8959.
42 Ionic Liquids Today-01-11.pdf from http://www.iolitec.de/en/Download-document/665-IonicLiquidsToday 01-11.pdf.html.
43 *Oxygen Chemistry*, ed. D. T. Sawyer, Oxford University Press, New York/Oxford, 1991.
44 R. S. Nicholson and I. Shain, *Anal. Chem.*, 1964, **36**, 706–723.

45 W. W. Lee, H. S. White and M. D. Ward, *Anal. Chem.*, 1993, **65**, 3232–3237.
46 R. M. Lynden-Bell, A. I. Frolov and M. V. Fedorov, *Phys. Chem. Chem. Phys.*, 2012, **14**, 2693–2701.
47 R. Hayes, N. Borisenko, M. K. Tam, P. C. Howlett, F. Endres and R. Atkin, *J. Phys. Chem. C*, 2011, **115**, 6855–6863.
48 M. Z. Bazant, B. D. Storey and A. A. Kornyshev, *Phys. Rev. Lett.*, 2011, **106**, 046102.
49 S. J. Martin, V. E. Granstaff and G. C. Frye, *Anal. Chem.*, 1991, **63**, 2272–2281.
50 P. Bonhôte, A.-P. Dias, N. Papageorgiou, K. Kalyanasundaram and M. Grätzel, *Inorg. Chem.*, 1996, **35**, 1168–1178.
51 P. Hapiot and C. Lagrost, *Chem. Rev.*, 2008, **108**, 2238–2264.